Journal of the Air & Waste Management Association
Publication details, including instructions for authors and subscription information:
http://www.tandfonline.com/loi/uawm20

Estimating surface visibility at Hong Kong from ground-based LIDAR, sun photometer and operational MODIS products

Muhammad I. Shahzad [a b], Janet E. Nichol [a], Jun Wang [b], James R. Campbell [c] & Pak W. Chan [d]

[a] The Hong Kong Polytechnic University, Department of Land Surveying and Geo-Informatics, Hung Hom, Hong Kong

[b] University of Nebraska, Department of Earth and Atmospheric Sciences, Lincoln, NE, USA

[c] Naval Research Laboratory, Monterey, CA, USA

[d] Hong Kong Observatory, Kowloon, Hong Kong

Accepted author version posted online: 13 May 2013.Published online: 20 Aug 2013.

To cite this article: Muhammad I. Shahzad, Janet E. Nichol, Jun Wang, James R. Campbell & Pak W. Chan (2013) Estimating surface visibility at Hong Kong from ground-based LIDAR, sun photometer and operational MODIS products, Journal of the Air & Waste Management Association, 63:9, 1098-1110, DOI: 10.1080/10962247.2013.801372

To link to this article: http://dx.doi.org/10.1080/10962247.2013.801372

TECHNICAL PAPER

Estimating surface visibility at Hong Kong from ground-based LIDAR, sun photometer and operational MODIS products

Muhammad I. Shahzad,[1,2,*] Janet E. Nichol,[1] Jun Wang,[2] James R. Campbell,[3] and Pak W. Chan[4]

[1]*The Hong Kong Polytechnic University, Department of Land Surveying and Geo-Informatics, Hung Hom, Hong Kong*
[2]*University of Nebraska, Department of Earth and Atmospheric Sciences, Lincoln, NE, USA*
[3]*Naval Research Laboratory, Monterey, CA, USA*
[4]*Hong Kong Observatory, Kowloon, Hong Kong*
[*]*Please address correspondence to: Muhammad I. Shahzad, Department of Land Surveying and Geo-Informatics, The Hong Kong Polytechnic University, Hung Hom, Hong Kong; e-mail: imran.shahzad@connect.polyu.hk*

Hong Kong's surface visibility has decreased in recent years due to air pollution from rapid social and economic development in the region. In addition to deteriorating health standards, reduced visibility disrupts routine civil and public operations, most notably transportation and aviation. Regional estimates of visibility solved operationally using available ground and satellite-based estimates of aerosol optical properties and vertical distribution may prove more effective than standard reliance on a few existing surface visibility monitoring stations. Previous studies have demonstrated that such satellite measurements correlate well with near-surface optical properties, despite these sensors do not consider range-resolved information and indirect parameterizations necessary to solve relevant parameters. By expanding such analysis to include vertically resolved aerosol profile information from an autonomous ground-based lidar instrument, this work develops six models for automated assessment of surface visibility. Regional visibility is estimated using co-incident ground-based lidar, sun photometer, visibility meter, and MODerate-resolution maging Spectroradiometer (MODIS) aerosol optical depth data sets. Using a 355 nm extinction coefficient profile solved from the lidar, MODIS AOD (aerosol optical depth) is scaled down to the surface to generate a regional composite depiction of surface visibility. These results demonstrate the potential for applying passive satellite depictions of broad-scale aerosol optical properties together with a ground-based surface lidar and zenith-viewing sun photometer for improving quantitative assessments of visibility in a city such as Hong Kong.

Implications: The study presents methods to estimate surface level visibility using remote sensing techniques, thus reducing the cost and effort required to estimate visibility at regional level. This helps to address environmental and health effects of ambient air pollution related to visibility for areas with no existing air quality monitoring stations. Policy regulation and hazard assessments impacting transportation and navigation can be improved by integrating the remotely estimated surface visibility with a real-time environmental data network.

Introduction

Hong Kong's skyline and mountain horizons are obscured 20% of the time due to reduced visibility (visual range [VR] below 8 km; e.g., Chang and Koo, 1986; Lai and Sequeira, 2001). The percentage of hours with such reduced visibility (excluding fog, rain, or mist) has risen from 2% in 1970 to 18% in 2004 (Hong Kong Observatory [HKO], 2005). This is primarily the result of high aerosol particulate loading, with mean annual aerosol optical depth (AOD) values exceeding 0.60 at 550 nm (Wu et al., 2005). Air quality in urban Hong Kong is considered worse than in surrounding rural areas (Louie et al., 2005), and, for context, is worse than most urbanized coastal areas of eastern USA (Yuan et al., 2002).

Hong Kong's declining visibility is closely related to local and regional air pollution (Chan and Yao, 2008), as light extinction correlates strongly with concentrations of respirable suspended particles (RSPs; particles with diameter of less than 10 μm) within the planetary boundary layer (PBL) (Chin, 1997; Lee and Gervat, 1995; Sequeira and Lai, 1998). Optical properties of these aerosols depend on their emission source (Cui et al., 2011). Local anthropogenic activities, as well as aerosol particle transport, most commonly in the form of sulfate (SO_4) from neighboring China, are primary contributors (Cheung et al., 2005; Qun et al., 2009; Zhuang et al., 1999). Lai and Sequeira (2001) show that NO_2 and RSPs are responsible for 79% of light extinction in Hong Kong. In comparison, Wan et al., (2011) report a high correlation between visibility and PM_{10} (particulate matterwith an aerodynamic diameter $\leq$10 μm) when the latter decreases by 0.004 mg/m^3 and with NO_2 when NO_2 decreases from 0.02 to 0.05 mg/m^3 in the nearby Pearl River Delta (PRD) region during 2001 to 2008. Deteriorating visibility has

Journal of the Air & Waste Management Association, 63(9):1098–1110, 2013. ISSN: 1096-2247 print
DOI: 10.1080/10962247.2013.801372

prompted concern for health as well as transportation, aviation, and other routine civil operations (Thach et al., 2010).

Several methods are available for surface-based measurements of horizontal VR, including human operator estimates (Hyslop, 2009), transmissometer (Horvath, 1981), nephelometer (Horvath and Kaller, 1994), teleradiometer (Watson, 2002; William, 1999), aerosol speciation and parameterized estimates (Malm et al., 1994; Jung et al., 2009; Bian, 2011), the use of digital cameras (Bäumer et al., 2008), and use of linear regression of turbidity as function of air mass (Peterson et al., 1981). Almost all of these methods are difficult to deploy, maintain, and operate over a large region (Babari et al., 2011). In Hong Kong, surface VR is measured operationally at five locations in and around Hong Kong's main islands by qualified weather observers, forward scatterering radiometers, and transmissometers. This includes an urban site, managed by the Hong Kong Observatory (HKO; at 22.301°N, 114.174°E) across Victoria Harbor, and in the outer suburbs at the Hong Kong International Airport (HKIA; at 22.309°N, 113.922°E; Figure 1). Although these monitoring sites have contributed a number of new and important data sets for better characterizing the problem, they are not sufficient to cover all of Hong Kong. Also, such estimates are representative only of a specific sample of space or direction, and cannot be presumed representative of adjacent regions (Anderson et al., 2003).

Efforts have been reported to supplement surface networks with satellite remote sensing to estimate surface level atmospheric VR (Kaufman and Fraser, 1983; Hadjimitsis et al., 2010). Satellite remote sensing has been shown to improve such efforts by using one or a combination of approaches. Some relevant examples include (1) the use of solar albedo for deriving geometric and optical thickness of fog from Advance Very High Resolution Radiometer (AVHRR; Mishchenko et al., 2003) and sonic detection and ranging (SODAR), including a radiative transfer model for calculating the extinction coefficient (Bendix, 1995); (2) the use of luminance and contrast from satellite image in spatial and frequency domains derived from radiative transfer models (Diner, 1985; Williams and Cogan, 1991); (3) atmospheric transmittance derived from satellite AOD measurements (Hadjimitsis et al., 2010; Nichol et al., 2010); and (4) the use of statistical regressions with different combinations of band radiances to estimate VR (Fei et al., 2006). However, these studies focus only on stratified layers of fog, and all lack appropriate validation measurements for very clear or highly polluted (i.e., high AOD) days/cases. Therefore, their use for a highly polluted region like Hong Kong is untested.

Furthermore, passive aerosol remote sensors do not resolve aerosol distributions vertically with reliably high resolution (in the order of 1–100 m), whereas space-borne lidar instruments, of which the National Aeronautics and Space Administration (NASA) Cloud Aerosol Lidar with Orthogonal Polarization instrument (CALIOP; Winker et al., 2010) is currently the only operational sensor, do offer this measurement. However, CALIOP's limited sensor swath width and orbital track makes these data difficult to apply practically in a routine/daily operational setting relative to other passive sensors. Instead, we consider the opportunity to combine the benefits of regional passive satellite aerosol observations with surface-based lidar profiling to better constrain local VR estimates.

Therefore, in this study, the vertical profile of aerosol particle scattering and distribution is estimated from a single-channel elastic-scattering lidar at Hong Kong Polytechnic University (HKPU; at 22.30°N, 114.197°E). Six algorithms are then described and tested, where regional VR is estimated using coincident ground-based lidar, sun photometer, and AOD data sets of the Moderate-resolution maging Spectroradiometer (MODIS; Ackerman et al., 1998). Using the 355 nm extinction coefficient

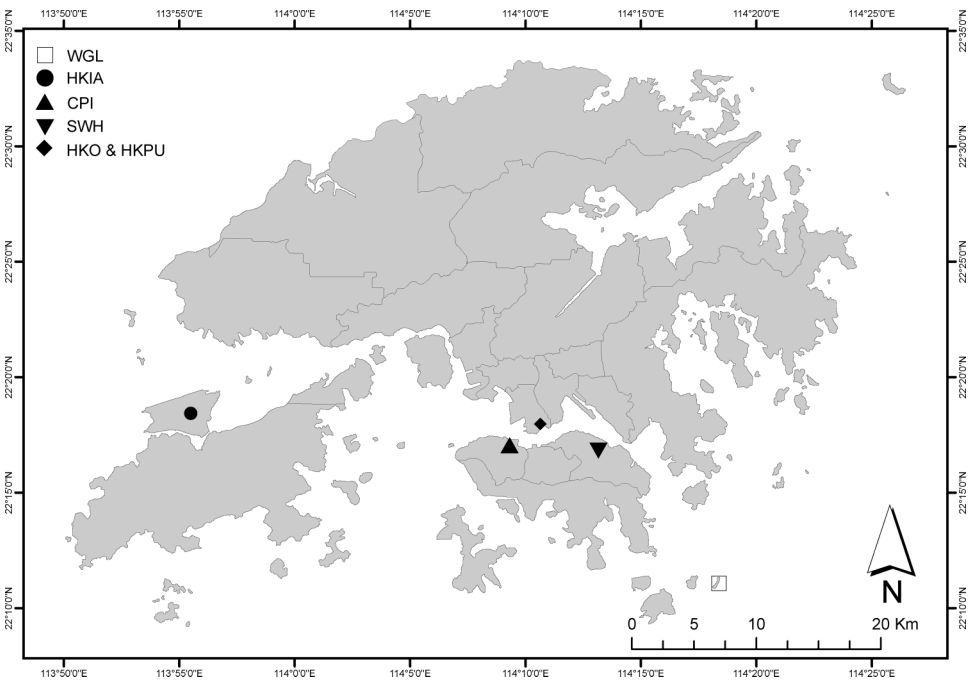

Figure 1. Locations of the visibility monitoring stations in Hong Kong (HKO and HKPU are 0.5 km apart).

profile derived from the lidar measurements at one location, MODIS AOD data are scaled down to the surface to generate a regional composite depiction of surface VR. We assume the vertical distribution of aerosol particle mass concentration over the Hong Kong study domain is constant relative to its horizontal distribution. We evaluate this assumption by comparing our results with independent VR measurements at locations where lidar data do not exist. By applying this technique, it is possible to optimize information from a relatively limited number of available ground visibilities to estimate VR across the entire area from passive remote sensing data sets, which provide the necessary spatial coverage.

Research Tools

Study area

The Hong Kong domain studied here represents an aggregate surface area of 1104 km^2, located in a subtropical region surrounded by the South China Sea to the east, south, and west, and bordering Shenzhen, China, to the north. The maximum altitude above mean sea level (MSL) is 957 m and approximately 40% of the land area is preserved as country park lands. Hong Kong experiences local as well as regional transboundary air pollution. In the warm summer months, southwesterly winds bring fresh marine air, resulting in a relatively clean, hot, and humid atmosphere (Cheng et al., 2006). From October to April, cold air masses from South China transport regional pollutants (Cheng et al., 2006), making air quality poor. Local visibility is highest in the hot humid summer, with southerly winds from South China Sea, and lowest in the winter and spring, with dry northerly winds from continental China (Chang and Koo, 1986; Mui et al., 2009).

Data used

This study considers hourly average data sets collected with a 355 nm elastic scattering lidar instrument, a multichannel sun photometer, deployed as part of NASA's federated Aerosol Robotic Network (AERONET; Holben et al., 1998), and a visibility meter (Vaisala, Finland), all installed on the urban campus of HKPU at 22.30°N, 114.197°E. Data are evaluated from April 2011, beginning with the availability of routine lidar observations at HKPU, through October 2011, corresponding with the availability of quality-assured Level 2 AERONET products that are cloud screened as well as pre- and post-field calibrated. However, in order to sample a larger number of MODIS data for validating our method, we extend the study period beyond October 2011 to September 2012 using only Level 1.5 AERONET data, which are cloud screened but without a final postoperation calibration applied. Overall, though, only six data points were used from Level 1.5 data of AERONET for our validation study.

MODIS. MODIS was first launched on the Terra satellite in 1999 in a descending node that passes the equator at 1030 local time. A second MODIS, on the Aqua platform, was launched in 2001 in an ascending node, which passes the equator at 1:30 p.m. local time. With 36 wavebands at 250 m, 500 m, and 1 km resolution, MODIS can be used for atmospheric, oceanic, and land studies at both local and global scales (e.g., Remer et al., 2005; Wong et al., 2011). The MODIS Science Team generates specific value-added data products describing aerosol physical and optical properties, including ocean color, land cover, and fire locations (Schaaf et al., 2002; Moody et al., 2008). The current MODIS operational products (MOD04—from Terra and MYD04—from Aqua), with 10 km horizontal resolution, represent Collection 5 (Levy et al., 2007). The AOD from MOD04 and MYD04 are extracted for the HKPU (τ_{MU}) and HKIA (τ_{MA}) sites using spatial windows of 5 × 5 pixels, which are then compared with hourly average values of data from AERONET, the lidar, and visibility meter. These temporal and spatial windows were designed in accordance with Anderson et al. (2003), who report a significant correlation ($r > 0.90$) between AOD measurements from ground, air, and space using a temporal window of less than 3 hr and a spatial window of less than 60 km.

AERONET data. The AERONET sun photometer database includes AOD over a range of wavelengths (0.35–1.05 μm), with an accuracy of ±0.015 (Rainwater and Gregory, 2005). Instruments are generally calibrated annually. Typically, measurements are collected and reported at 15 min resolution. Value-added Level 2 products (i.e., aside from AOD) include aerosol single-scattering albedo, size distribution, fine and coarse mode fractions, phase function, and asymmetric function (Dubovik and King, 2000). AERONET data are widely used for the validation of satellite AOD retrievals and model simulations (Yu et al., 2003).

We note recent work suggesting that Level 2 AERONET screening algorithms may be limited by optically thin cirrus clouds, most common in tropical and subtropical locales, thus leading to a positive-definite AOD bias of 0.03–0.06 when such clouds go unscreened (Chew et al., 2011). In Singapore, for instance, this can approach 35% of the Level 2 sample. In this study, however, we apply the Level 2 archive directly and presume the cloud-screening procedures are robust. Despite the presence of lidar measurements, during daytime, when the passive radiometric observations used here are available, the Atmospheric Lidar System (ALS; Lolli et al., 2011) proves insensitive to cloud presence at heights and temperatures most commonly associated with optically thin tropical cirrus. Thus, no consideration of potential cloud bias in the AERONET sample is possible.

LIDAR data. The ALS at HKPU collects data at 15 m and 1 min spatial and temporal resolutions, respectively. The ALS is a single-channel elastic backscatter lidar, operated at 355 nm, with an outgoing energy pulse near 16 μJ at 20 Hz. The ALS data used in this study do not account for Rayleigh scattering and gas and particle absorption. Signals are processed for a relative backscattering coefficient (β; $m^{-1}sr^{-1}$), which can be interpreted for significant aerosol particle layers, such as the surface-detached mixed aerosol layer (referred to as mixing layer—low; ML-Low) and diffuse elevated layers decoupled from the primary surface layer and advecting within the free troposphere (ML-High). Further processing can yield an estimated extinction coefficient (σ_{LS}; m^{-1}), where AOD (τ_{LU}) is either constrained and extinction solved iteratively through an inversion solution to the lidar equation (Fernald, 1984; Klett, 1985), or by setting the relationship between extinction and backscatter coefficients constant within an assumed turbid layer and again constraining total

transmission to solve extinction bin-by-bin from the top of the layer to the surface.

In this work, the latter technique for solving the extinction is applied using built-in software provided by the ALS manufacturer, which includes a predefined set of extinction-to-backscatter ratios. The extinction-to-backscatter ratio can fluctuate depending on the region of interest, particularly in Southeast Asia (Campbell et al., 2012). At Hong Kong, it is found to fluctuate seasonally between 18 and 44 sr at 532 nm (He, 2006). This led us to choose a value ratio of 36 sr (e.g., Ackerman et al., 1998), thus reflecting urban pollution as the primary aerosol type regionally. Note that overlap of the ALS system is achieved at a range approximating 170 m. Thus, in order to estimate near-surface VR effectively, we use data as close to the surface as possible and extrapolate downward (described below). Therefore, the hourly average extinction coefficient (σ_{LU}) at 355 nm is retrieved from the LIDAR measurements at heights between 75 and 150 m.

Surface visibility data. A Vaisala visibility meter is collocated with the sun photometer and lidar at HKPU. This meter uses a forward-scattering method to estimate visual range at 875 nm. Intensity of infrared light scattered at 33° is measured and converted to VR. VR readings from this station (V_{HKPU}) are used below to construct model estimates. VR readings from a similar visibility meter deployed at HKIA (V_{HKIA}) are used for validation. Human observations of visibility are also important for such a study but could not be used, as none were available for HKPU.

Descriptive statistics

Histograms depicting hourly averages of the parameters (V_{HKPU}, V_{HKIA}, ML-High, ML-Low, σ_{LU}, τ_{AU}, and τ_{LU}) used by the various models for estimating VR are shown in Figure 2. Log-normal distributions are observed in all except for ML-High, V_{HKPU}, and V_{HKIA}, which exhibit bimodal distributions. Summary statistics for these hourly averages, including sample size, mean, median, standard deviation, and maximum/minimum values, are given in Table 1. The highest values for ML-High and ML-Low during the study period were 2.82 and 2.51 km, respectively. The lowest values were 0.36 and 0.23 km, respectively. On average, the majority of aerosol particles were present within a finite layer near the surface. This is suggested by the observation that ML-High (ML-Low) remained below 1 km 31.01% (60.01%) of the time. The average value of σ_{LU} was 0.22 km^{-1}, with maximum (minimum) values of 0.72 km^{-1} (0.16 km^{-1}) that correspond to VR of 5.43 km (24.45 km) according to Koschmieder's equation. Although τ_{LU} and τ_{AU} exhibit log-normal distributions, the lidar-derived AOD, which is based on

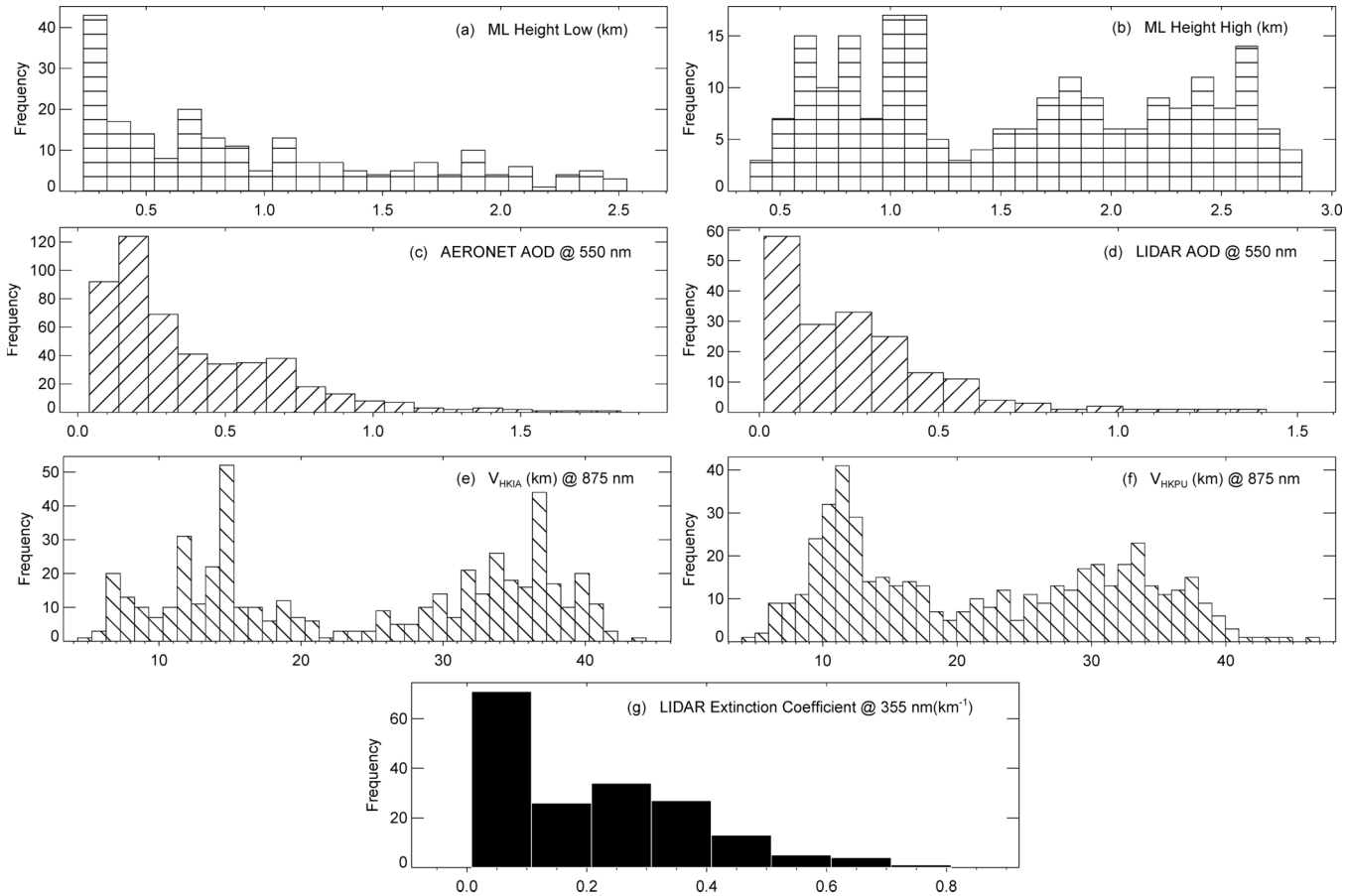

Figure 2. Frequency distribution hourly averages of (a) ML-Low, (b) ML-High, (c) AOD from AERONET, (d) AOD from ALS, (e) visibility at HKIA, (f) visibility at HKPU, and (g) extinction coefficient from ALS for height between 75 and 150 m.

Table 1. Summary statistics for hourly averages of visibility, LIDAR AOD, AERONET AOD, extinction coefficient, and ML heights presenting sample size (*N*), mean, median, standard deviation (SD), and maximum/minimum (Max/Min)

Parameter	*N*	Mean	Median	SD	Max	Min
V_{HKPU} at 875 nm (km)	489	21.77	20.82	10.41	46.17	3.965
V_{HKIA} at 875 nm (km)	492	24.28	25.79	11.39	44.03	4.28
τ_{LU} at 550 nm	183	0.28	0.23	0.24	1.41	0.01
τ_{AU} at 550 nm	492	0.39	0.28	0.30	1.80	0.04
σ_{LU} at 335 nm (km^{-1})	181	0.22	0.19	0.16	0.72	0.008
Z_H (km)	216	1.56	1.55	0.72	2.82	0.36
Z_L (km)	216	0.97	0.76	0.64	2.51	0.23

Notes: Z_H = ML-High; Z_L = ML-Low.

an assumption of constant extinction-to-backscatter ratio, was low compared with AERONET retrievals. Average values of τ_{LU} and τ_{AU} were 0.28 and 0.39, respectively. These smaller values of τ_{LU} can be reconciled by using eq 4 to represent V_{HKPU}.

We note that VR between 20 and 30 km was more frequent than VR below 20 km or above 30 km for both HKIA and HKPU. The peak frequency at HKPU was ∼11−12, and that at HKIA was ∼15 and standard deviation and mean values for V_{HKPU} and V_{HKIA} are significantly different (*P* value = 0.00), with values of V_{HKPU} and V_{HKIA} of 21.77 ± 10.41 and 24.28 ± 11.39 km, respectively. This supports our assumption of spatial variability of aerosol mass concentrations in Hong Kong.

Scatter plots of V_{HKPU} versus σ_{LU}, τ_{LU}, ML-Low, τ_{AU}, and V_{HKIA} are shown in Figure 3, and each shows significant correlation (*P* values <0.05), thus indicating the relevance of applying these parameters to estimate VR. Studies involving the light extinction properties of aerosol particles have shown similarly good correlations (R^2 = 0.82–0.85) between ML height and AOD when ML height is relatively low (Liu et al., 2009; Zieger et al., 2011) and the atmosphere is relatively stable. As noted by Xue et al (2010), light scattering increases as the height of the ML decreases because a lower ML reduces the volume of the air containing aerosol particles. Thus, increasing the aerosol loading per unit volume and hence the scattering of light. This likely explains the positive correlation (*R* = 0.70) observed for V_{HKPU} with ML-Low. Therefore, ML height can be approximated as a scaling height. A possible inverse relationship for V_{HKPU} and σ_{LU}, τ_{LU}, and τ_{AU} occurs, since an increase in the aerosol concentration increases the scattering and absorption. This results in increased extinction of light and hence decreases visibility, which has been shown in various studies over Hong Kong (e.g., Wang et al., 2003; Chan and Yao, 2008; Nichol et al., 2010; Wan et al., 2011). The

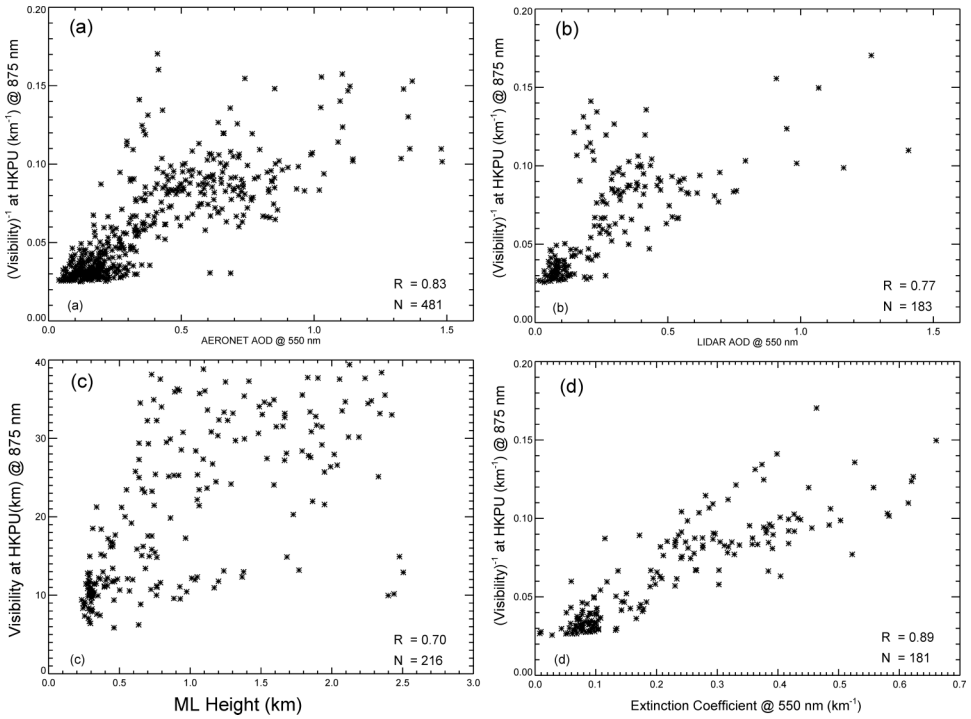

Figure 3. Relationship between visibility at HKPU derived from visibility meter at the 875 nm wavelength and (a) AOD from AERONET, (b) AOD from ALS, (c) ML-Low, and (d) extinction coefficient from ALS for height between 75 and 150 m at HKPU. Here *R* is correlation and *N* is the number of data points.

difference in the number of data points for ML heights, σ_{LU}, and τ_{LU} derived from ALS is due to the use of a constant extinction-to-backscatter ratio. This setting caused some retrievals to fail, which is a likely reflection of its true variance over time. Hence, τ_{LU} and σ_{LU} were not retrieved for every day.

Methodology

ALS extinction coefficient profiles

Although ALS data are collected at 15 m and 1 min resolution, integrated profiles can improve the signal-to-noise ratio (SNR) (e.g., Campbell et al., 2008). Therefore, hourly averages of the extinction coefficient profile at 75 m resolution were computed. The arithmetic mean ($\sigma(t,r)$) and standard deviation ($\Delta\sigma(t,r)$) for each 1 min and 15 m profile were first computed after resolving the profile to 75 m resolution (i.e., 5 bin averages at 15 m resolution). Next, the hourly average of 75 m and 1 min extinction coefficient profiles was derived by computing, once again the arithmetic mean of each 75 m and 1 min profile available in an hour (eq 1). The relative uncertainty in the hourly averaged profile was then computed using eq 2.

$$\sigma_{LU}(t,r) = \frac{\sum_{t=0}^{t=59} \sigma_t(r)}{N} \quad (1)$$

$$\Delta\sigma_{LU}(t,r) = \frac{\sqrt{\sum_{t=0}^{t=59} [\Delta\sigma_t(r)]^2}}{N} \quad (2)$$

Here, N is the total number of profiles in an hour and σ_{LU} and $\Delta\sigma_{LU}$ are the hourly averaged profiles of extinction coefficient and their corresponding relative uncertainty at 75 m resolution. Ratio of eqs 1 and 2 give the SNR for the corresponding profile, as

$$\mathrm{SNR}(r) = \frac{\sigma_{LU}(r)}{\Delta\sigma_{LU}(r)} \quad (3)$$

To extract a representative ALS surface extinction coefficient (scaled surface extinction coefficient, σ_S, at 355 nm) from signals measured within the overlap region of the lidar, some correction or scaling is necessary due to possible uncertainty corresponding to the overlap region and use of a static ratio of extinction and backscatter (as described above) of 36 sr. To overcome this problem, the ratio of τ_{AU} to τ_{LU} are used in order to constrain the lidar equation and scale σ_S relative to AERONET as

$$\sigma_S = \frac{\tau_{AU}}{\tau_{LU}} \times \sigma_{LU}(\mathrm{at}\, r = 75\,\mathrm{m}) \quad (4)$$

where σ_{LU} is reported at 355 nm. Note here that τ_{AU} and τ_{LU} are scaled up to 550 nm using corresponding values of Ångstrom exponent ($\alpha_{440\,nm-675\,nm}$ and $\alpha_{340\,nm-500\,nm}$) from the AERONET Level 2 data sets, since τ_{AU} and τ_{AU} are measured at 500 and 355 nm from AERONET and ALS, respectively.

Nonlinear regression analysis

It is assumed that σ_S and V_{HKPU} will exhibit an inverse empirical relationship, in a form similar to Koschmieder's law (Koschmieder, 1924), that can be applied to the entire Hong Kong domain under our assumption of constant and persistent aerosol vertical distributions. Therefore, a formula is proposed to estimate V_{HKPU} using σ_S as

$$V_{HKPU} = \frac{a}{\sigma_S + b} \quad (5)$$

where a (unitless) and b (km^{-1}) are constants that can be estimated using a non-linear regression fit between σ_S and V_{HKPU}. The values of parameters a and b will be different from the 3.912 and 0.0 km^{-1} prescribed by Koschmieder's equation, which correspond to an assumed visual contrast of (0.02) and extinction of light due to gases as well as particles, whereas σ_S accounts for extinction of light due to particles in air only. Also, V_{HKPU} accounts for scattering due to particles only. Hence, values of a and b also account for absorption due to NO_2 as well as brown and black carbon, which are important contributors to visibility reduction in an urban atmosphere.

Modeled extinction coefficient

As noted in the previous section (Figure 2e and f), there is significant spatial variability in VR between HKIA and HKPU, such that a measurement of VR in one location cannot be representative of another location. Therefore, in this study six models are developed (Table 2) to use MODIS data to spatially extrapolate either σ_{LU} measurements (Models 1–3) or VR measurements (Models 5–6) at HKPU to the HKIA. MODIS data are used to account for the spatial variability in VR and it is assumed that this reduces uncertainty in the extrapolation of VR measured in one location to another. Also, since errors are reported in MODIS and LIDAR data, it is not known if inclusion of these

Table 2. Proposed models for estimating extinction coefficient of MODIS at HKIA (σ_{MA}) and V_{HKIA}

Model 1	$\sigma_{MA} = \frac{\tau_{MA}}{\tau_{LU}} \times \sigma_{LU}$
Model 2	$\sigma_{MA} = \frac{\tau_{MA}}{\tau_{AU}} \times \sigma_{LU}$
Model 3	$\sigma_{MA} = \frac{\tau_{MA}}{\tau_{MU}} \times \sigma_{LU}$
Model 4 (a and b)	$\sigma_{MA} = \frac{\tau_{MA}}{Z_{(L,H)}}$
Model 5	$V^{mod}_{HKIA} = \frac{\tau_{MA}}{\tau_{MU}} \times V_{HKPU}$
Model 6	$V^{mod}_{HKIA} = \frac{\tau_{MA}}{\tau_{AU}} \times V_{HKPU}$
Model 7	$V_{HKIA} = V_{HKPU}$

Notes: σ_{MA} = MODIS extinction coefficient of at HKIA
τ_{MA} = MODIS AOD at HKIA
τ_{MU} = MODIS AOD at HKPU
τ_{AU} = AERONET AOD at HKPU
τ_{LU} = LIDAR AOD at HKPU
$Z_{(L,H)}$ = Low- and High-ML heights at HKPU
V_{HKPU} = VR from visibility meter at HKPU
V_{HKIA} = VR from visibility meter at HKIA.

data adds useful information to the estimates. To evaluate the usefulness of the MODIS data in estimating VR, a "reference model" (Model 7) is also developed where VR at HKIA and HKPU are compared.

Models 1–4 estimate MODIS-derived surface level extinction coefficient (σ_{MA}) at 355 nm by using AOD and VR from the HKPU ground station along with MODIS data at HKIA and HKPU (τ_{MA}—MODIS AOD at HKIA and τ_{MU}—MODIS AOD at HKPU; each included in Table 1). Models 1–3 use AOD from the ALS and sun photometer along with σ_{LU} to compute σ_{MA}. However Model 4 uses only ML heights retrieved from the lidar to scale the MODIS AOD and simultaneously compute the near-surface extinction coefficient. This is reasonable since on average the majority of AOD measured at Hong Kong is the result of particle scattering below ML-Low (He et al., 2008; Campbell et al., 2012). Similar to eq 5, σ_{MA} from Models 1–4 is used to estimate V_{HKIA}^{mod} at 875 nm wavelength as

$$V_{HKIA}^{mod} = \frac{a}{\sigma_{MA} + b} \quad (6)$$

where values of a and b are the same as in eq 5. As mentioned above, eq 5 uses σ_S at 355 nm to derive V_{HKPU} at 875 nm. Therefore, σ_{MA} should also be at 355 nm. Hence, σ_{MA} from Model 4 was also scaled to 355 nm using Ångstrom exponent values from AERONET.

To study the effect of possible uncertainties involved in retrieval of ALS products due to use of a constant extinction to backscatter ratio, Models 5 and 6 were developed to be independent of the lidar. They use AOD and V_{HKPU} reported at wavelengths of 550 and 875 nm, respectively, and they directly report V_{HKIA}^{mod} at 875 nm without involving eqs 4 and 5. Equation 5 and all models are based on data from HKPU, and all are validated using data at HKIA. This allows an independent validation of algorithm performance at HKIA using in situ VR (V_{HKIA}).

Results and Discussion

Model fitting

A nonlinear regression model was fit to the data (eq 5) for the relationship between V_{HKPU} and σ_S (Figure 4). The value of the first parameter, a, is approximately 2 times greater than that prescribed by Koschmieder's equation (8.02 compared with 3.912). Koschmieder's values assume a visual contrast threshold of the eye at 0.02, where absorption and scattering of the optical medium correspond to the 500 nm wavelength. However, two of the terms in eq 5 are derived at different wavelengths: the σ_S in eq 5 is derived at the ultraviolet 355 nm wavelength and visibility at HKPU (V_{HKPU}) is derived from a forward scattering instrument, considering only scattering in the infrared region at 875 nm. Additionally, the calculated values for a comply with the fact that for a given particle with single-scattering albedo of 1 (SSA = 1), the scattering cross-section can increase significantly (Hansen and Travis, 1974) (i.e., approx. 2 times in the case of SO_4—a major pollutant reported for Hong Kong; Cheung et al., 2005; Qun et al., 2009; Zhuang et al., 1999) when the wavelength is changed from 550 to 335 nm. A lager value of b (of 0.2 km^{-1}) is also observed in the model, which may have one or two possible causes, including the extinction of light due to absorption by gases and particles, or due to the regression analyses which are based on least squares regression. This does not account for errors in the dependent variable, i.e., V_{HKPU}, which will result in overestimated intercept value, i.e., b. The fitting of the model with V_{HKIA} was able to explain only 50% of the variability in V_{HKPU}, possibly due to the use of the lidar extinction coefficient from the overlap region where reliability may be an issue (Kovalev and Eichinger, 2004).

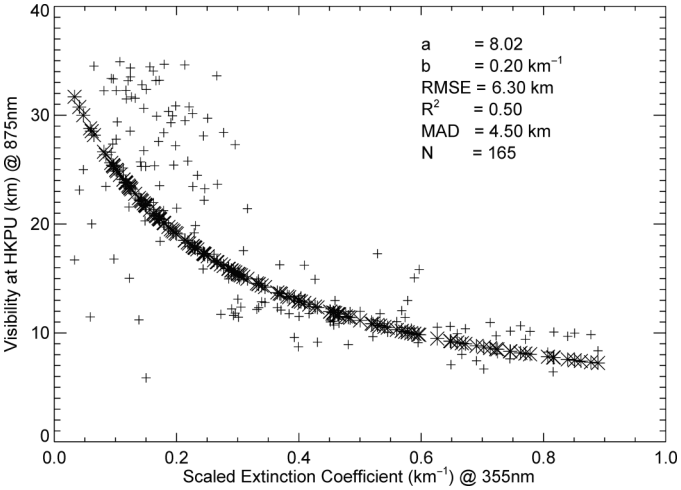

Figure 4. Nonlinear regression fit for scaled extinction coefficient and visibility at HKPU. Estimated values of the regression coefficients a and b and N are reported along with root mean square error (RMSE), mean absolute deviation (MAD), and coefficient of determination (R^2) for 165 measured values of visibility at HKPU and scaled surface extinction coefficient.

Validation

Regression coefficients a and b from eq 5 were used to estimate the modeled VR for Models 1–4, whereas Models 5–6 (Table 2) report the modeled VR alone. Each model requires a valid retrieval of MODIS AOD over HKIA. For the entire study period, there were only 46 suitable MODIS images, and only 14 of these (8 from 2011 and 6 from 2012) could be matched to concurrent lidar data for validation. The models were tuned using data from only HKPU. Modeled VR for those 14 days along with visibility meter readings at HKIA are shown in Figure 5. The error bars for V_{HKIA} correspond to the 20% expected uncertainty of the visibility meter (from its manual), which is consistent with Annex 3 of the International Civil Aviation Organization (ICAO) that suggests that an uncertainty of ±20% in estimated VR is acceptable when actual VR is above 1.5 km.

Models 2 and 3 give the best estimate of surface visibilities, followed by Models 5 and 6. Most of the models based on data from HKPU are able to reproduce variations in V_{HKIA}. This suggests that the models devised for Hong Kong provide reliable VR estimates without any bias for clear and polluted days, whereas previous studies (Diner, 1985; Fei et al., 2006; Otterman, 1985; Williams and Cogan, 1991) have overestimated and underestimated those conditions respectively. In fact, the

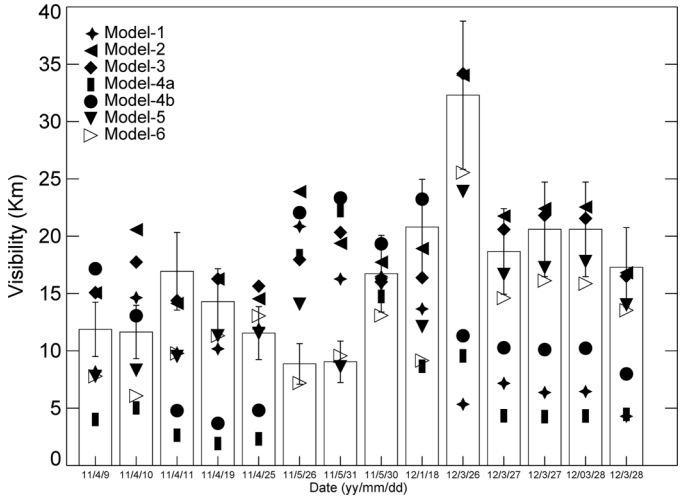

Figure 5. MODIS derived modeled visibility at HKIA from the proposed models listed in Table 1 and actual visibility (histogram bars) from visibility meter at HKIA. In addition to MODIS AOD, Model 1–4 uses AOD, ML heights, as well as extinction coefficients from ground-based instruments at HKPU, whereas Models 5 and 6 use visibility readings from visibility meter at HKPU. Error bars are ±20% of the visibility at HKIA from the manual of visibility meter.

modeled visibilities from Models 2, 3, 5, and 6 all fall within 1 standard deviation (6.17 km) of V_{HKIA} for validation days.

Model 1 underestimates VR most of the time, primarily because AOD estimates from the ALS are found to be biased low relative to AERONET. This is the reason that when τ_{AU} replaces τ_{LU} in Model 2, the modeled VR is fairly close to V_{HKIA} for most days. A similar argument is also valid for Model 3, whose performance is similar to Model 2.

Models 4a and 4b underestimate V_{HKIA} most of time. There are two primary reasons for this. The first is that the atmosphere was not well mixed for days with underestimated modeled VR. The second is that Models 4a and 4b depend on ML heights estimated from the ALS at HKPU. ML heights were derived from the lidar extinction profile based on a constant extinction-to-backscatter ratio, and we have seen that τ_{LU} is lower than τ_{AU}. Hence, the retrieved vertical distribution of AOD from ALS will also be lower and this influences the computation of ML. Results for Models 4a and 4b may suggest that underestimated ML heights caused overestimation in corresponding σ_{MA} and hence decrease the modeled VR.

It is noted that Models 1–4 are unable to estimate VR on 26 May 2011 and 31 May 2011 when V_{HKIA} is much lower than on other days. Also, Models 1 and 4 underestimate V_{HKIA} for most days, which are thought to be due to uncertainties associated with ALS data. Therefore, Models 5 and 6, which are independent of ALS data, were introduced, as they isolate the effect of possible uncertainties in σ_{LU} because both depend on AOD from MODIS and AERONET along with surface VR at HKPU. Both gave estimated V_{HKIA} better than Models 2 and 3. In addition, Model 6 was also able to estimate V_{HKIA} for both 26 May 2011 and 31 May 2011, whereas Model 5 was only able to estimate V_{HKIA} for 31 May 2011, in addition to other days. No other model was able to estimate V_{HKIA} for 26 May 2011 and 31 May 2011. Hence, the highest correlation between modeled and ground visibilities is found for these two models (Figure 6), which, overall, are best able to reproduce variations of V_{HKIA}.

Further assessments of the respective models are shown by scatter plots of modeled VR versus ground VR estimated at HKIA (Figure 6). VR estimates using Models 5 and 6 are concentrated closest to the 1:1 line. Hence, if we rank the models based on R^2, R, root mean square error (RMSE), and mean absolute deviation (MAD), Model 5 performs best, followed by Models 6 and 3.

Model results greatly improve (Table 3) if we remove 26 May 2011 and 31 May 2011 from the validation, based on unusually low values of V_{HKIA} corresponding to low MODIS AOD for these anomalous days at HKIA. MODIS AOD for these 2 days was 0.18 (0.17) and 0.20 (0.35), respectively, at HKIA (HKPU), whereas AERONET AOD was 0.33 and 0.32, respectively, at HKPU. Values of τ_{MA} and V_{HKIA} are low for these days relative to σ_{MU} and V_{HKPU}. This shows unusually low visibilities at HKIA when τ_{MA} was also low. Comparing values of R^2, R, RMSE, and MAD, Model 3 replaces Model 5 as the strongest performer. Again, the only difference between Models 3 and 5 (Table 1) is the use of surface extinction from the ALS. This once again shows that better-quality lidar data can result in better estimates of surface VR.

From Table 1, Models 4a and 4b depend on concurrent values of ML heights and MODIS AOD, whereas Model 5 and 6 depend on concurrent values of V_{HKPU} and MODIS AOD. Therefore, being independent of τ_{MU} and σ_{LU}, a larger validation data set for Models 4–6 can be arranged separately. Hence, Models 4–6 were further analyzed using respective extended validation data sets with corresponding numbers of data points (N) of 16, 16, 28, and 29, respectively (Figure 7). Model 5 still shows the best result, followed by Model 6. This demonstrates the robustness of the respective models. For a region where the vertical spatial distribution of aerosol physical properties can be considered constant, Models 3 and 5 are more applicable. Therefore, passive satellite remote sensing has the potential to estimate the surface VR to within an uncertainty of 20%, or that prescribed for a relatively simple visibility meter.

Although HKIA and HKPU are 35 km apart, there is a significant difference in the visibilities at these locations (Figures 2e, f and 6h). This suggests that a very dense ground-based visibility monitoring network is necessary in order to monitor the visibility of the entire Hong Kong domain. This is the reason that the reference model (Model 7) was unable to represent VR at HKIA (Figure 6). Models 2, 3, 5, and 6 using MODIS data performed better than the reference model, which indicates that inclusion of MODIS data is necessary for estimating VR at regional level. It also shows the merits of the proposed methods for estimating VR. Hence, passive satellite remote sensing techniques can be applied to optimize the use of a ground-based network and to fill gaps where no instruments are deployed. This will potentially help in reducing costs in monitoring regional air quality, since VR estimates can be used as a surrogate for mass concentration of fine particulates ($PM_{2.5}$; PM with an aerodynamic diameter $\leq$2.5 μm) (Chow et al., 2002; Vajanapoom et al., 2001).

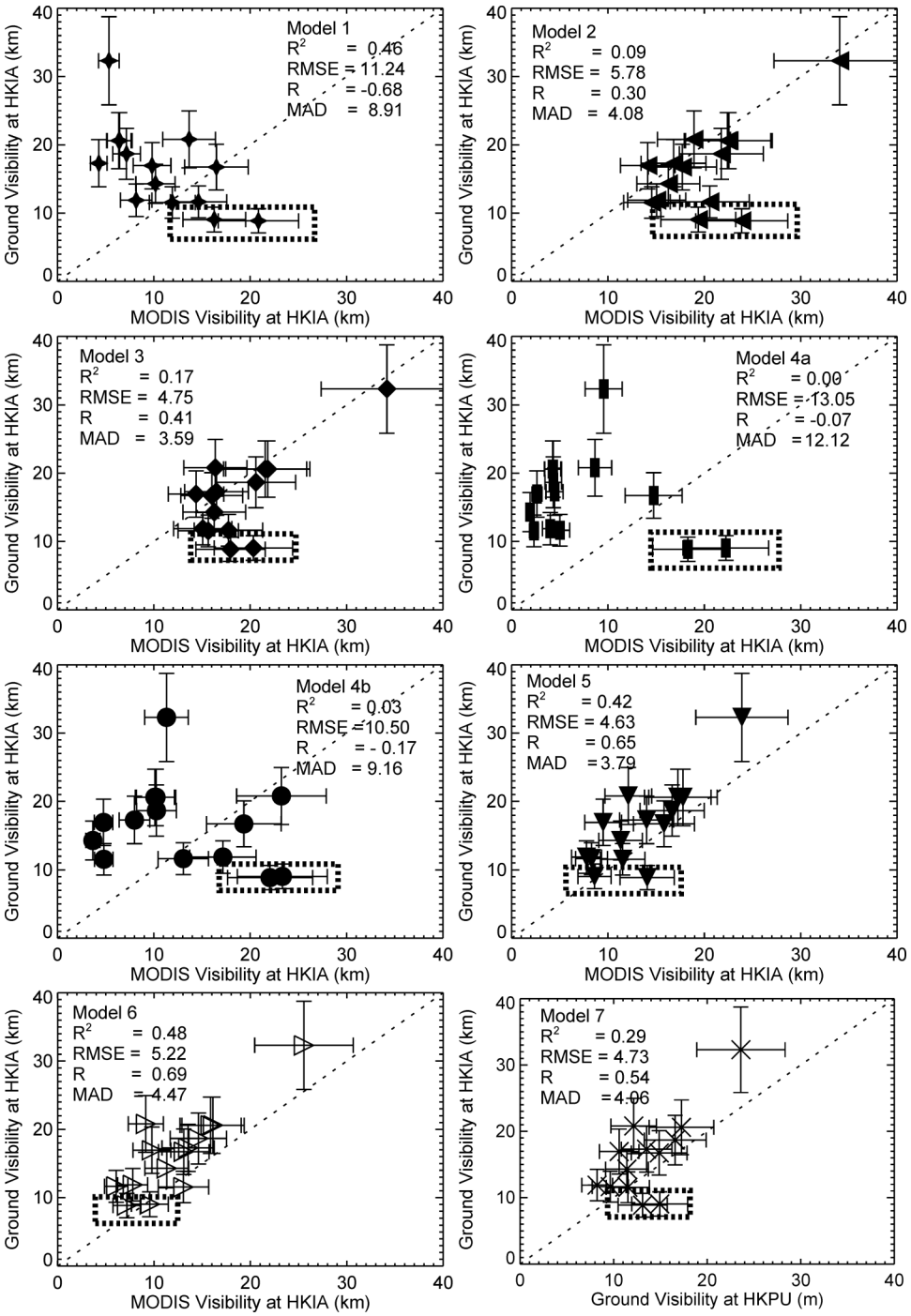

Figure 6. Scatter plot of V_{HKIA} and MODIS derived visibility at HKIA for each proposed model (Table 1). Dashed line displays the 1:1 line and dashed rectangle encompasses the data for 26 May 2011 and 31 May 2011. R^2, RMSE, and MAD are described in Figure 4.

Model selection

The predictive power of a model is indicated by the uncertainties in its inputs as well as the deviation of its output from actual values. It is good to note that the outputs of the proposed models are within ±20% of the ground values. However, uncertainties in the input parameters applied have reduced the performance of some models. Input parameters with the highest uncertainties can be attributed to the lidar data, and the use of a static extinction-to-backscatter ratio, necessary for estimating extinction, and the scaling of signal to the surface due to optical overlap of the instrument. In contrast, AOD from AERONET is considered to have the least uncertainty, although we again stress that the potential impact of optically thin cloud contamination of these data, and MODIS for that matter, was not considered, due to the limited profiling range during daytime of the ALS. VR measurements from the visibility meter are also prone to uncertainty, since they do not consider light absorption factors. However, the primary

Table 3. Comparison of model's performances before and after removal of data for 26 May 2011 and 31 May 2011

	Before Removal				After Removal			
Model	R^2	RMSE	R	MAD	R^2	RMSE	R	MAD
Model 1	0.46	11.24	−0.68	8.91	0.28	11.45	−0.53	8.80
Model 2	0.09	5.78	0.30	4.08	0.49	3.35	0.70	2.65
Model 3	0.17	4.75	0.41	3.59	*0.44*	*2.96*	*0.66*	*2.48*
Model 4a	0.00	13.05	−0.07	12.12	0.22	13.29	0.46	12.25
Model 4b	0.03	10.50	−0.17	9.16	0.05	9.85	0.22	8.40
Model 5	*0.42*	*4.63*	*0.65*	*3.79*	0.59	4.77	0.77	3.95
Model 6	0.48	5.22	0.69	4.47	0.49	5.61	0.63	5.03
Model 7	0.29	4.73	0.54	4.06	0.59	4.67	0.77	3.89

Note: Italicized values represent those of the best model.

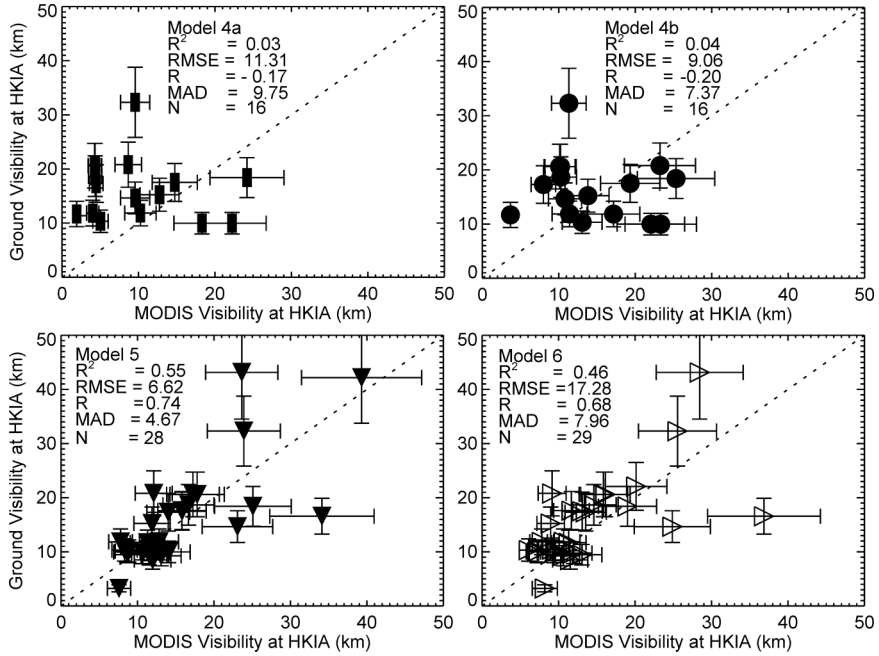

Figure 7. Scatter plot of V_{HKIA} and MODIS derived visibility at HKIA for Models 4–6 with extended validation data sets. Dashed line displays the 1:1 line. R^2, RMSE, and MAD are described in Figure 4 and N is the available number of data points for validation.

source of uncertainty involved in the estimation of VR in our models is due to the error term corresponding with the nonlinear regression step, since it is found to explain only 50% of the variations in σ_S and V_{HKPU}. A larger data set of σ_S and V_{HKPU} is needed to further improve the regression fitting.

To further the skill of the proposed models, a Taylor diagram (Taylor, 2001) was built (Figure 8). Taylor diagrams depict a statistical summary of how well patterns of estimated and observed values match based on their correlation, standard deviation, and root mean square error. The radial distance from the origin at "0.0" represents the normalized standard deviation. "Obs" represents the statistics of observed visibilities at HKIA. RMS differences for the modeled visibilities are proportional to the radial distances from the origin at "Obs" (units same as normalized standard deviation). Normalized Pearson's correlations between observed and modeled visibilities are represented along the azimuthal position along the outer hemisphere. The color bar scales the bias (%) in each model.

Pattern statistics describing the six modeled visibilities compared with observed visibilities at HKIA show that Models 2, 3, 5, and 6 outperform Models 1, 4a and 4b. The correlations for Models 5 and 6 are higher than for Models 2 and 3, whereas normalized standard deviations for Models 2, 3, and 6 are similar and higher for Model 5. Models 2 and 3 can be improved by using ALS data of better quality. However, the percentage biases for Models 5 and 3 are less than for Models 2 and 6. Overall, Model 5 appears to be the best model for the estimation of VR using MODIS AOD at HKPU and HKIA, along with VR from HKPU (Figure 8). Performance of these models is expected to further improve by retrieving AOD from MODIS at a high spatial resolution such as 3×3 km^2, which is planned for MODIS Collection 6 products (Levy et al., 2013).

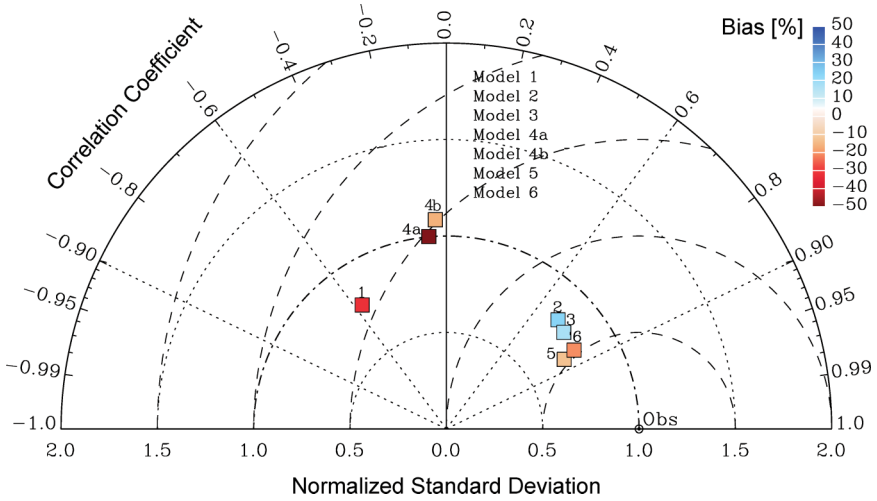

Figure 8. Pattern statistics (Taylor diagram; Taylor, 2001) describing the visibilities from the six models compared with observed visibilities at HKIA. The radial distance from the origin at "0.0" represents the normalized standard deviation. "Obs" represents the statistics of observed visibilities at HKIA. RMS difference for the modeled visibilities is proportional to the radial distances from origin at "Obs" (units same as normalized standard deviation). Normalized Pearson's correlation between observed and modeled visibilities is represented along the azimuthal position along the outer hemisphere. Color bar scales the normalized bias (%) in each model (color figure available online).

Conclusion

Deteriorating visibility at Hong Kong due to increase in regional air pollution raises concerns for local air quality and health standards. Existing networks monitoring local visibility are not sufficient. Therefore, this study was designed to model and estimate of VR using column-integrated aerosol physical properties from MODIS, ground-based lidar, and AERONET sun photometer measurements of aerosol optical depth. Six models are developed under the assumption that the vertical distribution of aerosol physical properties for the study domain is constant regionally on any particular day, but that the aerosol amount may vary spatiotemporally and the shape of aerosol vertical profile may vary temporally. Results suggest that models utilizing satellite observations together with the near-surface extinction coefficient from a visibility meter and ALS deployed at HKPU are reliable to estimate the VR 35 km away at HKIA.

VR estimates from the proposed models were found to be within 20% of ground values. The models did not overestimate or underestimate VR for clean and/or polluted days, as exhibited by previous studies of visibility modeling. Results may be further improved by model tuning and experience with a larger data set and over a longer study period. Results of the study demonstrate the potential for applying passive satellite depictions of broad-scale aerosol optical properties, and suggest that passive remote sensing exhibits the potential for enhancing the performance of preexisting ground-level visibility networks. Further, the integration of data from only one ground station and satellite images enables the estimation of surface level VR for an area up to 35 km away from the station, which is within reasonable spatiotemporal correlation lengths for aerosol optical properties evaluated previously (Anderson et al., 2003).

Results of this study can help devise methodologies for governments to more efficiently estimate VR at regional level. In addition to improvement in estimation of VR, this work can also lead to better understanding of environmental and health effects due to ambient air quality in terms of atmospheric visibility for areas with no existing air pollution monitoring stations. The integration of the remotely estimated VR into a real-time database network, such as Infusing Satellite Data into Environmental Applications (IDEA) by National Oceanic and Atmospheric Administration (NOAA) and Environment/ Environmental Central Facility (ENVF) Environmental and Atmospheric Database in Hong Kong, can help civil authorities both in improving policy regulation and for control of transportation and navigation. With that in mind, our continuing goal is to facilitate the implementation and further testing of such infrastructure in order to meeting the growing air quality-related issues faced by one of the world's largest metropolitan cities.

Acknowledgment

The authors would like to acknowledge the NASA Goddard Earth Science Distributed Active Archive Center for the MODIS Level IB and Level 2 data and Brent Holben for helping with the Hong Kong Polytechnic University AERONET station. Author M.S. kindly acknowledges Zhifeng Yang and Xiaoguang Xu at University of Nebraska–Lincoln for assisting in the analyses. M.S. also thanks Prof. David K. Watkins and the Department of Earth & Atmospheric Sciences for providing office space and other logistic help during his visit in UNL. The Hong Kong Polytechnic University Grant GYJ76 sponsored this research.

References

Ackerman, S.A., K.I. Strabala, W.P. Menzel, R.A. Frey, C.C. Moeller, and L.E. Gumley. 1998. Discriminating clear sky from clouds with MODIS. *J. Geophys. Res.* 103(D24):32141–32157. doi:10.1029/1998JD200032

Anderson, T.L., S.J. Masonis, D. S. Covert, N.C. Ahlquist, S.G. Howell, A.D. Clarke, and C.S. McNaughton. 2003. Variability of aerosol optical properties derived from in situ aircraft measurements during ACE-Asia. *J. Geophys. Res.* 108(D23ACE):15–19. doi:10.1029/2002JD003247

Babari, R., N. Hautière, É. Dumont, R. Brémond, and N. Paparoditis. 2011. A model-driven approach to estimate atmospheric visibility with ordinary cameras. *Atmos. Environ.* 45:5316–5324. doi:10.1016/j.atmosenv.2011.06.053

Bäumer, D., S. Versick, and B. Vogel. 2008. Determination of the visibility using a digital panorama camera. *Atmos. Environ.* 42:2593–2602. doi:10.1016/j.atmosenv.2007.10.017. xxx (accessed 24 January 2012).

Bendix, J. 1995. Determination of fog horizontal visibility by means of NOAA-AVHRR. *Quantitative Remote Sensing for Science and Applications* 3:1847, 1849. doi:10.1109/IGARSS.1995.524045

Bian, Q. 2011. Study of visibility degradation over the Pearl River delta region: Source apportionment and impact of chemical characteristics. Ph.D. dissertation, The Hong Kong University of Science and Technology, Hong Kong.

Campbell, J.R., J.S. Reid, D.L. Westphal, J. Zhang, J.L. Tackett, B.N. Chew, E.J. Welton, A. Shimizu, N. Sugimoto, K. Aoki, and D.M. Winker. 2012. Characterizing the vertical profile of aerosol particle extinction and linear depolarization over Southeast Asia and the Maritime Continent: The 2007–2009 view from CALIOP. *Atmos. Res.* 122:520–543. doi:10.1016/j.atmosres.2012.05.007

Campbell, J.R., K. Sassen, and E.J. Welton. 2008. Elevated cloud and aerosol layer retrievals from micropulse lidar signal profiles. *J. Atmos. Ocean. Technol.* 25:685–700. doi:10.1175/2007JTECHA1034.1

Chan, C.K., and X. Yao. 2008. Air pollution in mega cities in China. *Atmos. Environ.* 42:1–42. doi:10.1016/j.atmosenv.2007.09.003

Chang, W.L., and E.H. Koo. 1986. A study of visibility trends in Hong Kong (1968–1982). *Atmos. Environ.* 20:1847–1858. doi:10.1016/0004-6981(86)90325-2

Cheng, A.Y. S., M.H. Chan, and X. Yang. 2006. Study of aerosol optical thickness in Hong Kong, validation, results, and dependence on meteorological parameters. *Atmos. Environ.* 40:4469–4477. doi:10.1016/j.atmosenv.2006.04.022

Cheung, H.C., T. Wang, K. Baumann, and H. Guo. 2005. Influence of regional pollution outflow on the concentrations of fine particulate matter and visibility in the coastal area of southern china. *Atmos. Environ.* 39:6463–6474. doi:10.1016/j.atmosenv.2005.07.033

Chew, B.N., J.R. Campbell, J.S. Reid, D.M. Giles, E.J. Welton, S.V. Salinas, and S.C. Liew. 2011. Tropical cirrus cloud contamination in sun photometer data. *Atmos. Environ.* 45:6724–6731. doi:10.1016/j.atmosenv.2011.08.017

Chin, H.C. P. 1997. *Visibility Impairment in Hong Kong*. Hong Kong: Environmental Protection Department of Hong Kong.

Chow, J.C., J.G. Watson, D.H. Lowenthal, and L.W. Richards. 2002. Comparability between $PM_{2.5}$ and particle light scattering measurements. *Environ. Monit. Assess.* 79:29–45. doi:10.1023/A:1020047307117.

Cui, G.M., M. Zhang, Z. Han, and Y. Liu. 2011. Episode simulation of Asian dust storms with an air quality modeling system. *Adv. Atmos. Sci.* 28:511–520. doi:10.1007/s00376-010-0091-3

Diner, D. 1985. Influence of aerosol scattering on atmospheric blurring of surface features. *IEEE Trans. Geosci. Remote Sens.* GE-23:618–624. doi:10.1109/TGRS.1985.289379

Dubovik, O., and D.K. Michael. 2000. A flexible inversion algorithm for retrieval of aerosol optical properties from sun and sky radiance measurements. *J. Geophys. Res.* 105(D16):20673–20696. doi:10.1029/2000JD900282

Fei, H., W. Hong, Q. Junping, and W. Guofu. 2006. Retrieval of atmospheric horizontal visibility by statistical regression from NOAA/AVHRR satellite data. *J. Ocean Univ. China* 5:207–212. doi:10.1007/s11802-006-0003-4

Fernald, F. 1984. Analysis of atmospheric lidar observations: Some comments. *Appl. Opt.* 23:652–653. doi:10.1364/AO.23.000652

Hadjimitsis, D.G., C. Clayton, and L. Toulios. 2010. Retrieving visibility values using satellite remote sensing data. *Phys. Chem Earth A/B/C* 35:121–124. doi:10.5194/nhess-10-89-2010

Hansen, J.E., and L.D. Travis. 1974. Light scattering in planetary atmospheres. *Space Sci.* Rev. 16:527–610. doi:10.1007/BF00168069

He, Q.S. 2006. A study on aerosol extinction-to-backscatter ratio with combination of micro-pulse lidar and MODIS over Hong Kong. *Atmos. Chem. Phys. Discuss.* 6:3099–3133. doi:10.5194/acpd-6-3099-2006

He, Q., C. Li, J. Mao, A.K.H. Lau, and D.A. Chu. 2008. Analysis of aerosol vertical distribution and variability in Hong Kong, *J. Geophys. Res.* 113 (D14): D14211.1–D14211.13, doi:10.1029/2008JD009778

Holben, B.N., T.F. Eck, I. Slutsker, D. Tanré, J.P. Buis, A. Setzer, E. Vermote. 1998. AERONET—A federated instrument network and data archive for aerosol characterization. *Remote Sens. Environ.* 66:1–16. doi:10.1016/S0034-4257(98)00031-5

Hong Kong Observatory. Press release. 2005. http://www.hko.gov.hk/wxinfo/news/2005/pre0106e.htm (accessed October 29, 2012).

Horvath, H. 1981. The university of Vienna telephotometer. *Atmos. Environ.* 15:2537–2546. doi:10.1016/0004-6981(81)90069-X.

Horvath, H., and W. Kaller. 1994. Calibration of integrating nephelometers in the post-halocarbon era. *Atmos. Environ.* 28:1219–1223. doi:10.1016/1352-2310(94)90299-2

Hyslop, N.P. 2009. Impaired visibility: The air pollution people see. *Atmos. Environ.* 43:182–195. doi:10.1016/j.atmosenv.2008.09.067

Jung, J., H. Lee, Y.J. Kim, X. Liu, Y. Zhang, J. Gu, and S. Fan. 2009. Aerosol chemistry and the effect of aerosol water content on visibility impairment and radiative forcing in Guangzhou during the 2006 Pearl River Delta campaign. *J. Environ. Manage.* 90:3231–3244. doi:10.1016/j.jenvman.2009.04.021

Kaufman, Y.J., and R.S. Fraser. 1983. Light extinction by aerosols during summer air pollution. *J. Climate Appl. Meteorol*. 22:1694–1706. doi:10.1175/1520-0450(1983)022<1694:LEBADS>2.0.CO;2

Klett, J.D. 1985. Lidar inversion with variable backscatter/extinction ratios. *Appl. Opt.* 24:1638–1643. doi:10.1364/AO.24.001638

Koschmieder, H. 1924. Theorie der horizontalen sichtweite. *Beitr. Phys. Frei. Atmos.* 12:33–171.

Kovalev, V.A., and W.E. Eichinger. 2004. *Elastic Lidar: Theory, Practice, and Analysis Methods*. Hoboken, NJ: John Wiley.

Lai, L.Y., and R. Sequeira. 2001. Visibility degradation across Hong Kong: Its components and their relative contributions. *Atmos. Environ.* 35:5861–5872. doi:10.1016/S1352-2310(01)00395-8

Lee, F.Y.P., and G.P. Gervat. 1995. *Visibility Degradation and Its Relationship to Air Quality.* Hong Kong: Environmental Protection Department of Hong Kong.

Levy, R.C., S. Mattoo, L.A. Munchak, L.A. Remer, A.M. Sayer, and N.C. Hsu. 2013. The Collection 6 MODIS aerosol products over land and ocean, *Atmos. Meas. Tech. Discuss.* 6:159–259. doi:10.5194/amtd-6-159-2013

Levy, R.C., L.A. Remer, S. Mattoo, E.F. Vermote, and Y.J. Kaufman. 2007. Second-generation operational algorithm: Retrieval of aerosol properties over land from inversion of moderate resolution imaging spectroradiometer spectral reflectance. *J. Geophys. Res.* 112(D13): 2–21. doi:10.1029/2006JD007811

Liu, P., C. Zhao, Q. Zhang, Z. Deng, M. Huang, X. Ma, and X. Tie. 2009. Aircraft study of aerosol vertical distributions over Beijing and their optical properties. *Tellus B* 61:756–767. doi:10.1111/j.1600-0889.2009.00440.x

Lolli, S., L. Sauvage, S. Loaec, and M. Lardier. 2011. EZ Lidar: A new compact autonomous eye-safe scanning aerosol Lidar for extinction measurements and PBL height detection. Validation of the performances against other instruments and intercomparison campaigns. *Opt. Pura Appl.* 44:33–41.

Louie, P.K., J.C. Chow, L.W. Chen, J.G. Watson, G. Leung, and D.W. Sin. 2005. $PM_{2.5}$ chemical composition in Hong Kong: Urban and regional variations. *Sci. Total Environ.* 338:267–281. doi:10.1016/j.scitotenv.2004.07.021

Malm, W.C., K.A. Gebhart, J. Molenar, T. Cahill, R. Eldred, and D. Huffman. 1994. Examining the relationship between atmospheric aerosols and light extinction at Mount Rainier and north cascades national parks. *Atmos. Environ.* 28:347–360. doi:10.1016/1352-2310(94)90110-4

Mishchenko, M.I., I.V. Geogdzhayev, L. Liu, J.A. Ogren, A.A. Lacis, W.B. Rossow, J.W. Hovenier, H. Volten, and O. Muñoz. 2003. Aerosol retrievals from AVHRR radiances: Effects of particle nonsphericity and absorption and an updated long-term global climatology of aerosol properties. *J. Quant. Spectrosc. Radiat. Transfer.* 79–80:953–972. doi:10.1016/S0022-4073(02)00331-X

Moody, E.G., M.D. King, C.B. Schaaf, and S. Platnick. 2008. MODIS-derived spatially complete surface albedo products: Spatial and temporal pixel

distribution and zonal averages. *J. Appl. Meteorol. Climatol.* 47:2879–2894. doi:10.1175/2008JAMC1795.1

Mui, K.W., L.T. Wong, and P.S. Hui. 2009. Screening strategies of an indoor air quality express assessment protocol (EAP) for air-conditioned offices. *Indoor Built Environ.* 18:77–82. doi:10.1177/1420326X08101529

Nichol, J.E., M.S. Wong, and J. Wang. 2010. A 3D aerosol and visibility information system for urban areas using remote sensing and GIS. *Atmos. Environ*. 44:2501–2506. doi:10.1016/j.atmosenv.2010.04.036

Otterman, J. 1985. Satellite measurements of surface albedo and temperatures in semi-desert. *J. Climate Appl. Meteorol.* 24:228–235. doi:10.1175/1520-0450(1985)024<0228:SMOSAA>2.0.CO;2

Peterson, J.T., E.C. Flowers, G.J. Berri, C.L. Reynolds, and J.H. Rudisill. 1981. Atmospheric turbidity over central North Carolina. *J. Appl. Meteorol. Climatol.* 20:229–241. doi:10.1175/1520-0450(1981)020<0229:ATOCNC>2.0.CO;2

Qun, L.S., L. Mang, W.J. Ming, C.C. Yu, and S.X. Fang. 2009. Characterization and relationship of long-term visibility and air pollutant changes in the Hong Kong region. *China Environ. Sci.* 29:351–356.

Rainwater, M., and L. Gregory. 2005. *Cimel Sun Photometer (CSPHOT) Handbook*. ARM TR-056, U.S. Department of Energy, Office of Science, Office of Biological and Environmental Research. http://www.arm.gov/instruments/

Remer, L.A., Y.J. Kaufman, D. Tanré, S. Mattoo, D.A. Chu, J.V. Martins, R.R Li. 2005. The MODIS aerosol algorithm, products and validation. *J. Atmos. Sci.* 62:947–973. doi:10.1175/JAS3385.1

Schaaf, C.B., F. Gao, A.H. Strahler, W. Lucht, X. Li, T. Tsang, N.C. Strugnell. 2002. First operational BRDF, albedo nadir reflectance products from MODIS. *Remote Sens. Environ.* 83:135–148. doi:10.1016/S0034-4257(02)00091-3

Sequeira, R., and K.H. Lai. 1998. The effect of meteorological parameters and aerosol constituents on visibility in urban Hong Kong. *Atmos. Environ.* 32:2865–2871. doi:10.1016/S1352-2310(97)00494-9

Taylor, E.K. 2001. Summarizing multiple aspects of model performance in a single diagram. *J. Geophys. Res.* 106:7183–7192. doi:10.1029/2000JD900719

Thach, T.Q., C.M. Wong, K.P. Chan, Y.K. Chau, Y.N. Chung, C.Q. Ou, L. Yang, and A.J. Hedley. 2010. Daily visibility and mortality: Assessment of health benefits from improved visibility in Hong Kong. *Environ. Res.* 110:617–623. doi:10.1016/j.envres.2010.05.005

Vajanapoom, N., C.M. Shy, L.M. Neas, and D. Loomis. 2001. Estimation of particulate matter from visibility in Bangkok, Thailand. *J. Expos. Anal. Environ. Epidemiol.* 11:97–102. doi:10.1038/sj.jea.7500148

Wan, J.M., M. Lin, C.Y. Chan, Z.S. Zhang, G. Engling, X.M. Wang, I.N. Chan, and S.Y. Li. 2011. Change of air quality and its impact on atmospheric visibility in central-western Pearl River delta. *Environ. Monit. Assess.* 172:339–351. doi:10.1007/s10661-010-1338-2

Wang, T., C.N. Poon, Y.H. Kwok, and Y.S. Li. 2003. Characterizing the temporal variability and emission patterns of pollution plumes in the Pearl River delta of China. *Atmos. Environ.* 37:3539–3550. doi:10.1016/S1352-2310(03)00363-7

Watson, J.G. 2002. Visibility: Science and regulation. *J. Air Waste Manage. Assoc.* 52:628–713. doi:10.1080/10473289.2002.10470813

William, C.M. 1999. *Introduction to Visibility.* Fort Collins, CO Cooperative Institute for Research in the Atmosphere, NPS Visibility Program, Colorado State University. http://www.epa.gov/visibility/pdfs/introvis.pdf.

Williams, D.H., and J.L. Cogan. 1991. Estimation of visibility from satellite imagery. *Appl. Opt.* 30:400–414. doi:10.1364/AO.30.000414

Winker, D.M., J. Pelon, J.A. Coakley, S.A. Ackerman, R.J. Charlson, P.R. Colarco, P. Flamant. 2010. The CALIPSO mission: A global 3D view of aerosols and clouds. *Bull. Am. Meteorol. Soc.* 91:1211–1229. doi:10.1175/2010BAMS3009.1.

Wong, M.S., J.E. Nichol, and K.H. Lee. 2011. An operational MODIS aerosol retrieval algorithm at high spatial resolution, and its application over a complex urban region. *Atmos. Res.* 99:579–589. doi:10.1016/j.atmosres.2010.12.015

Wu, D., X. Tie, C. Li, Z. Ying, A.K.H. Lau, J. Huang, X. Deng, and X. Bi. 2005. An extremely low visibility event over the Guangzhou region: A case study. *Atmos. Environ*. 39:6568–6577. doi:10.1016/j.atmosenv.2005.07.061.

Xue, M., F. Kong, K.W. Thomas, Y. Wang, K. Brewster, J. Gao, X. Wang, S.J. Weiss, A.J. Clark, J.S. Kain, M.C. Coniglio, J. Du, T.L. Jensen, and Y.H. Kuo. 2010. CAPS real time storm scale ensemble and high resolution forecasts for the NOAA hazardous weather test bed. 2010 spring experiment. In *25th Conference on Severe Local Storms, Denver, CO*, October 11, 2010, *American Meteorological Society*, Paper 7B.3.

Yu, H.B., R.E. Dickinson, M. Chin, Y.J. Kaufman, B.N. Holben, I.V. Geogdzhayev, and M.I. Mishchenko. 2003. Annual cycle of global distributions of aerosol optical depth from integration of MODIS retrievals and GOCART model simulations. *J. Geophys. Res.* 108(D3):1–14. doi:10.1029/2002JD002717

Yuan, C.S., C.G. Lee, S.H. Liu, C. Yuan, H.Y. Yang, and C.T.A. Chen. 2002. Developing strategies for improving urban visual air quality. *Aerosol Air Qual. Res.* 2:9–22. doi:10.4209/2002.06.0002

Zhuang, H., C.K. Chan, M. Fang, and A.S. Wexler. 1999. Size distributions of particulate sulfate, nitrate, and ammonium at a coastal site in Hong Kong. *Atmos. Environ.* 33:843–853. doi:10.1016/S1352-2310(98)00305-7.

Zieger, P., E. Weingartner, J. Henzing, M. Moerman, G. de Leeuw, J. Mikkilä, M. Ehn. 2011. Comparison of ambient aerosol extinction coefficients obtained from in-situ, MAX-DOAS and LIDAR measurements at Cabauw. *Atmos. Chem. Phys.* 11:2603–2624. doi:10.5194/acp-11-2603-2011

About the Authors

Muhammad I. Shahzad is a Ph.D. candidate at the Department of Land Surveying and Geo-Informatics, The Hong Kong Polytechnic University, Hung Hom, Hong Kong. Presently, he is a visiting research scholar at the Department of Earth and Atmospheric Sciences, University of Nebraska, Lincoln, Nebraska, USA.

Janet E. Nichol is a professor at the Department of Land Surveying and Geo-Informatics, The Hong Kong Polytechnic University, Hung Hom, Hong Kong.

Jun Wang is a professor at the Department of Earth and Atmospheric Sciences, University of Nebraska, Lincoln, Nebraska, USA.

James R. Campbell is a meteorologist assigned to the Aerosol and Radiation Section at the Naval Research Laboratory in Monterey, California, USA.

Pak W. Chan is a senior scientific officer at Hong Kong Observatory, Kowloon, Hong Kong.